Chinese Chemical Letters 37 (2026) 112307

Contents lists available at ScienceDirect

Chinese Chemical Letters

journal homepage: www.elsevier.com/locate/cclet

Heterostructured Janus covalent organic framework membranes *via* multiphase interfacial polymerization for unidirectional water transport and nanofiltration

Ya Lu[a,b], Chao Jia[a], Shu-Yan Jiang[a], Qiao-Yan Qi[a], Jin Yao[a,c,*], Xin Zhao[a,*]

[a] State Key Laboratory of Organometallic Chemistry, Shanghai Institute of Organic Chemistry, University of Chinese Academy of Sciences, Chinese Academy of Sciences, Shanghai 200032, China
[b] College of Chemistry and Material Science, Shanghai Normal University, Shanghai 200234, China
[c] School of Chemistry and Materials Science, Hangzhou Institute for Advanced Study, University of Chinese Academy of Sciences, Hangzhou 310024, China

ARTICLE INFO

Article history:
Received 9 September 2025
Revised 10 December 2025
Accepted 21 December 2025
Available online 23 December 2025

Keywords:
Multiphase interfacial polymerization
Covalent organic framework
Janus membrane
Asymmetric wettability
Unidirectional water transport

ABSTRACT

Herein, a multiphase interfacial polymerization strategy has been developed to controllably fabricate A-to-B type Janus covalent organic framework (COF) membranes with asymmetric properties. This approach allows one-pot construction of heterostructured COF membranes with opposite wettability on the upper and lower surfaces *via* integrating simultaneous but independent interfacial polymerizations at two interfaces of a three-phase system. Being integrated two distinct two-dimensional COF layers with the same frame structure but differing in side chains, the Janus COF membranes exhibits hydrophilic feature on one side but displays hydrophobic characteristic on the other side. Additionally, the Janus COF membranes exhibit exceptional anti-pollution performance and exclusively permits unidirectional water transport. Notably, this unique property is non-designable in the homogeneous COF membranes fabricated from the same building blocks *via* the conventional two-phase interfacial polymerization method. The Janus membranes were further demonstrated to be a good candidate for membrane desalination with a high rejection for $MgSO_4$. This novel multiphase interfacial polymerization strategy offers a general way to fabricate Janus membranes with designable, predictable, and controllable asymmetric properties from a wide range of materials, holding great potential for diverse applications.

© 2026 Published by Elsevier B.V. on behalf of Chinese Chemical Society and Institute of Materia Medica, Chinese Academy of Medical Sciences.

Surface wettability plays an important role in industrial processes and the natural world [1–5]. With their great application potentials in filtration and distillation, membranes with controlled surface wettability have recently drawn a lot of attention [6–9]. The function of membranes is closely linked to their fluid wetting behavior. However, traditional membranes exhibit homogeneous wetting behavior on both sides due to their symmetric surface wettability, thus limiting their performance in specific scenarios. For example, unidirectional fluid transport and selective liquid separation are hard to achieve with symmetric membranes alone [10,11]. In recent years, Janus membranes have emerged as a novel class of functional membranes, offering solutions to address these challenges, thanks to their distinctive asymmetric surface wettability [12–18]. As a result of the asymmetric characteristic, Janus membranes enable a wide range of distinctive fluid wetting features, such as unidirectional fluid transport and selective fluid separation [19–23]. The unique fluid transport behavior relies on the cooperative effects stemming from the asymmetric wettability across the membranes. So far, there are two primary methods for the fabrication of Janus membranes: Single-layer modification and double-layer composite. The former involves asymmetric surface modification of a membrane to create a Janus feature [24,25]. While this approach offers control over the specific wettability of membranes, it is usually limited by strict reaction types and conditions. On the other hand, the double-layer composite method concerns cementing two separately prepared membranes to produce an asymmetric membrane [26–28]. Although this approach is simpler than the surface modification, mismatched cementation might arise, resulting in increase of transport resistance. In this context, precise creation and regulation of asymmetry remains a key challenge in the development of Janus membranes.

In recent years, covalent organic frameworks (COFs), as a class of crystalline porous organic materials [29–31], have emerged as a new type of membrane materials with great potentials due to their precisely pre-designable pore structures and tailored func-

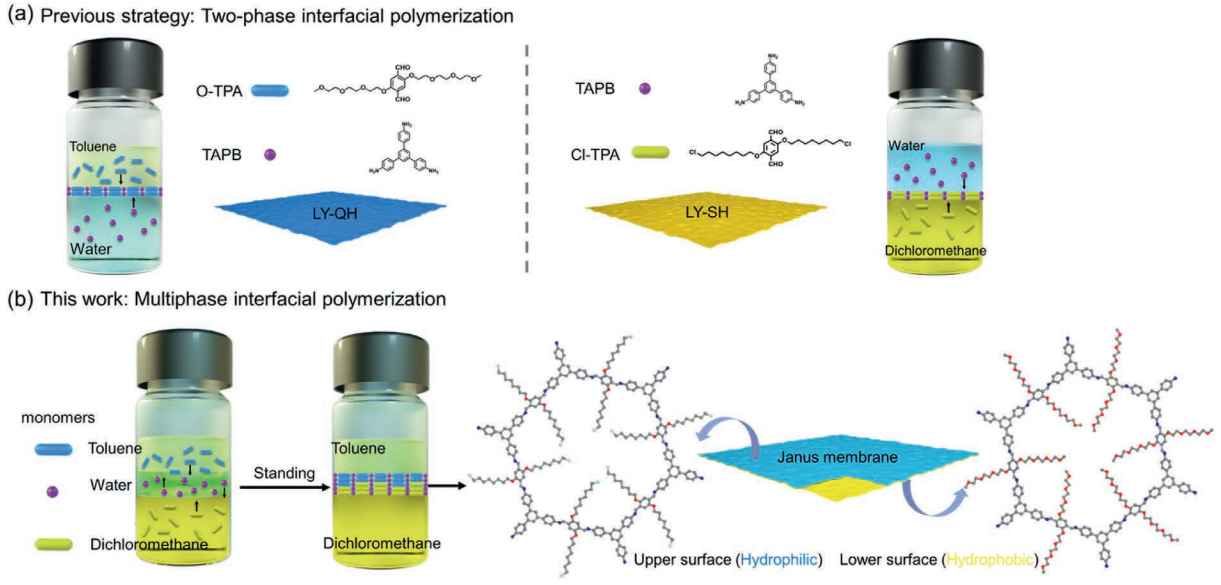
* Corresponding authors.
E-mail addresses: yaojin@ucas.ac.cn (J. Yao), xzhao@sioc.ac.cn (X. Zhao).

https://doi.org/10.1016/j.cclet.2025.112307
1001-8417/© 2026 Published by Elsevier B.V. on behalf of Chinese Chemical Society and Institute of Materia Medica, Chinese Academy of Medical Sciences.

tions [32–41]. To overcome the limitation that COFs are usually synthesized as insoluble and unprocessable powder, interfacial polymerization has been implemented for the fabrication of COF membranes [42–45]. In a typical process, monomers are dissolved separately in two immiscible phases, and a polymerization reaction takes place at their interface to produce a COF membrane over time. This strategy has achieved considerable success in construction of COF membranes [46–48]. However, it is hard to fabricate Janus membranes because both two sides of the as-formed membranes have the same composition. Although formation of Janus COF membranes *via* this approach was serendipitously observed, this phenomenon was not universal, and so far only a few cases have been reported [49,50]. In those cases, the difference in the membrane surfaces was attributed to different diffusion rates of the monomers. Since such a diffusion-controlled structural alteration is susceptible to environmental influences, it is non-designable and uncontrollable. To address this problem, we anticipated that a designable and controllable strategy for constructing asymmetric COF membranes should be based on chemical composition control, wherein components with different wettability could be introduced on-demand to the upper and lower surfaces of a membrane, respectively [51]. However, this strategy cannot be realized by the established two-phase interfacial polymerization. In this study, we have developed a method termed "multiphase interfacial polymerization" to solve this problem, by which designable, predictable, and controllable fabrication of Janus COF membranes with asymmetric wettability has been successfully achieved. COF membranes fabricated from two-phase and multiphase interfacial polymerization were compared side-by-side. Unique properties and higher application performance were observed for the Janus COF membranes fabricated by multiphase interfacial polymerization.

As depicted in Scheme 1, dialdehydes modified with hydrophobic alkyl side chains (Cl-TPA) and hydrophilic oligo(ethylene glycol) side chains (O-TPA) were dissolved in dichloromethane and toluene, respectively, which served as two oil phases. Additionally, a co-precursor, triamine (TAPB), was dissolved in water (with acetonitrile as an additive) to form an aqueous phase which locates between the two oil phases. By adjusting the quantity of water and the composition of the additive in the aqueous phase (see Supporting information for details), we successfully fabricated a Janus COF membrane (denoted as LY-Janus) with asymmetric wettability from a toluene-water-dichloromethane three-phase system. As observed, at the early stage of the multiphase interfacial polymerization process, two thin films initially formed at the toluene/water interface and water/dichloromethane interface *via* independent interfacial polymerizations between the amine monomer and the corresponding aldehyde monomers, respectively [45,52]. During the preparation of this manuscript [53], a triple-layer-dual interfacial approach was reported to independently synthesize two different 3D COF membranes [54]. Subsequently, the two polymerization processes continued as the two aldehyde monomers diffuse crossing from the films *via* opposite direction driven by concentration gradient. As a result, the two films grew thicker and thicker, and they became closer and closer to each other, with gradual outdiffusion of water. Finally, the two films merged each other to produce a monolithic three-component Janus membrane. For comparative purposes, two-component COFs membranes, one with hydrophobic alkyl side chains (LY-SH) and the other with hydrophilic oligo (ethylene glycol) side chains (LY-QH) were also prepared using the conventional two-phase interfacial polymerization method (see Supporting information for details) [55,56].

The as-obtained membranes were characterized with Fourier transform infrared (FT-IR) and solid-state cross-polarization magic angle spinning carbon-13 nuclear magnetic resonance (CP/MAS ^{13}C NMR) spectroscopy, which confirmed the formation of imine polymers. The comparison of FT-IR spectra of the membranes and their corresponding monomers revealed disappearance of the vibration peaks corresponding to N–H (3341 cm^{-1}) and C=O (1680 cm^{-1}) and appearance of C=N vibration band (1617 cm^{-1}) after the condensation reactions (Figs. S12-S14 in Supporting information) [57,58], indicating the formation of polyimine structures. Moreover, the FT-IR spectrum of LY-Janus looks like a superposition of the spectra of LY-SH and LY-QH (Fig. 1a), suggesting that it contains the constituents from both the two membranes. The formation of polyimines was also supported by solid-state ^{13}C CP/MAS NMR spectroscopy, which displays the characteristic signal of C=N at 153 ppm (Fig. 1b). Particularly, the comparison of their ^{13}C CP/MAS NMR spectra clearly indicates that the Janus COF membrane consists of the chemical components from both the monomers Cl-TPA and O-TPA, as evidenced by the co-appearance of the peaks corresponding to the alkyl chain (69, 45, 33, 30, and 28 ppm) and the oligo (ethylene glycol) segment (71 and 59 ppm) (Figs. S15-S17 in



Scheme 1. Schematic representation for the fabrication of COF membranes (represented by LY-QH and LY-SH) *via* the traditional two-phase interfacial polymerization and the Janus COF membrane (LY-Janus) *via* multiphase interfacial polymerization.

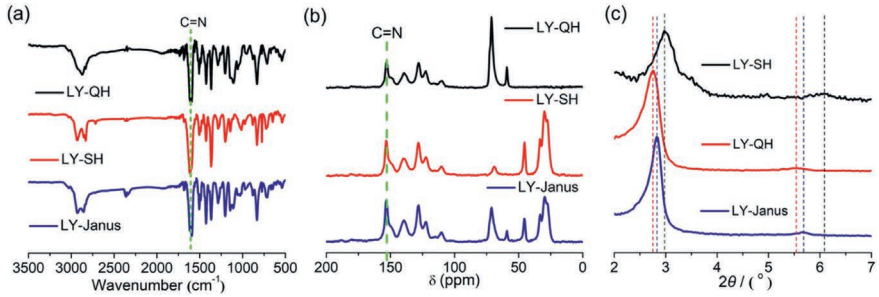


Fig. 1. Comparisons of (a) FT-IR and (b) solid-state CP/MAS ^{13}C NMR spectra, and (c) PXRD patterns of LY-SH, LY-QH, and LY-Janus.

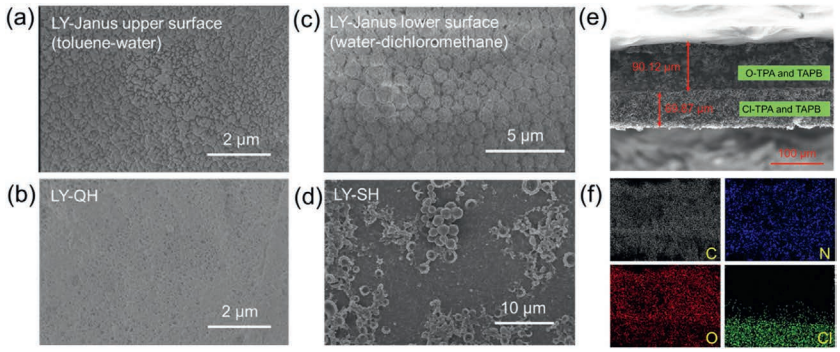


Fig. 2. (a-d) SEM images of the surfaces of LY-Janus, LY-QH, and LY-SH. (e) Cross-sectional SEM image of LY-Janus (fabricated from an O-TPA/Cl-TPA ratio of 2:1), and (f) cross-sectional EDX mapping image of LY-Janus.

Supporting information) [59,60]. Powder X-ray diffraction (PXRD) corroborated the crystallinity of the three COF membranes. And their crystal structures were elucidated on the basis of the experimental PXRD data and theoretical simulations (Figs. S18-S23 in Supporting information). A close comparison of the (100) diffraction peaks of the three membranes provides more information (Fig. 1c). Firstly, LY-SH and LY-QH display a slight but clear difference in the position of their (100) peaks, albeit they share the same framework skeleton. It could be attributed to their different side chains, for which the influence of substituents on the PXRD diffraction was observed in previous studies [61,62]. Secondly, the (100) peak of LY-Janus lies between the peaks of LY-SH and LY-QH, which is consistent with the fact that it contains both the frameworks of LY-SH and LY-QH, again corroborating the formation of the designed three-component COF membrane.

More characterization was carried out to disclose the microstructures and features of the COF membranes. Thermal gravimetric analysis (TGA) revealed that the membranes had good thermal stability (Fig. S24 in Supporting information). Nitrogen sorption measurements confirmed their porosity, with BET surface areas of 89, 135, and 244 m^2/g for LY-SH, LY-QH, and LY-Janus, respectively (Figs. S25-S27 in Supporting information). The low surface areas could be attributed to occupation of their pores by the long side chains. Moreover, their pore size distribution profiles indicate that they possess narrow distribution and very close pore sizes (around 24 Å) (Figs. S28-S30 in Supporting information), indicating well-ordered channels in the membranes. The surface morphology of the three membranes was investigated with scanning electron microscopy (SEM). As shown in the SEM images, the upper surface of LY-Janus displays a morphology of aggregated nanosheets (Fig. 2a), which closely resembles to the surface of LY-QH (Fig. 2b). This surface exhibits a huge roughness and dense texture, facilitating spreading of water droplets on the membrane surface. In contrast, the lower surface of LY-Janus shows a morphology of aggregated nanospheres (Fig. 2c), which is similar to the lower surface of the LY-SH membrane (Fig. 2d). We further employed atomic force microscopy (AFM) to assess the surface roughness of the membranes (Fig. S31 in Supporting information). 3D morphology images obtained by AFM revealed that the roughness of both the upper and lower surfaces of LY-Janus were comparable, with values of 27.8 nm and 24.2 nm, respectively, which is consistent with the roughness of the upper surface of LY-QH (32.9 nm) and the lower surface of LY-SH (24.9 nm). These results are in accordance with the predicted outcome of the growing procedure of LY-Janus. Moreover, the cross-sectional SEM image of the LY-Janus membrane clearly reveals distinct morphologies for the upper and the lower parts and their merging in the middle (Fig. 2e), further confirming that LY-Janus is formed by the coalescence of the two different COF membranes.

The cross-section of LY-Janus was further investigated by energy dispersive X-ray spectroscopy (EDX). Thanks to the introduction of chlorine in the hydrophobic alkyl side chains of the building block, its distribution in the membrane could be clearly identified by EDX. The elemental mapping demonstrates uniform distribution of C, N, and O across the whole cross-section, which is consistent with the fact that both LY-SH and LY-QH share the same framework consisting of C, N, and O. In contrast, a gradient decline in the content of chlorine was observed from the bottom surface to middle section (Fig. 2f). Depth-profiling XPS analysis was further carried out to elucidate the compositional distribution within the LY-Janus membrane. As the etching depth increased, the characteristic Cl signal gradually decreased, indicating that Cl-containing moieties are predominantly concentrated on the lower surface (Fig. S32 in Supporting information). The above results could be explained by the fact that the upper part mostly comes from LY-QH, whereas the lower parts is mainly consist of LY-SH, and the middle part is generated by the formation of COF solid solution from copolymerization of Cl-TPA, O-TPA, and TAPB [63]. Since dialdehydes Cl-TPA and O-TPA simultaneously diffused into the aqueous phase in opposite direction, it can be anticipated that they will coexist in the middle part, and the closer to the middle between the two interfaces, the more balanced distribution of Cl-TPA and O-TPA. This result also

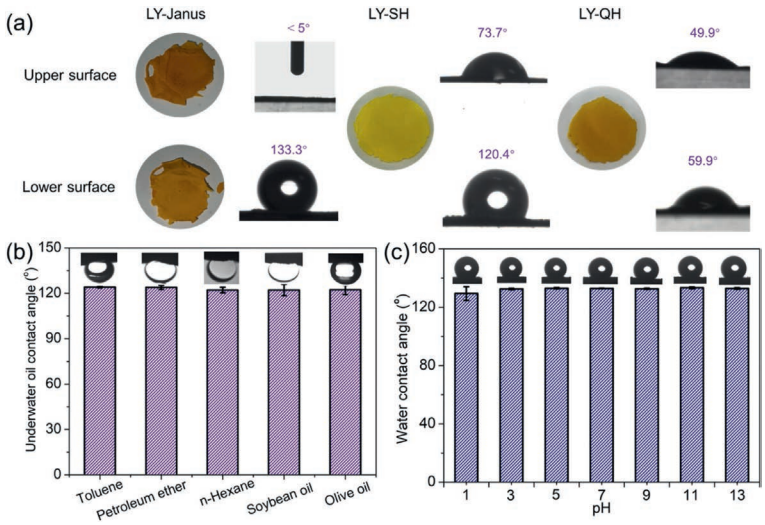


Fig. 3. (a) Water contact angles of upper and lower surface, (b) underwater oil contact angles at five types of oils, and (c) water contact angles at different pH values.

suggests the Janus COF membrane is integrated, with gradual transition of the two distinct COFs. On the other hand, this result also indicates a gradual change in wettability (or polarity) across the membrane thickness, that is, gradually shifting from hydrophilic to hydrophobic (or reverse). Such a hydrophilicity gradient feature was found to play a crucial role in improving performance of membrane distillation [64]. Furthermore, the thickness of the upper and lower COF membranes in LY-Janus could be tuned by adjusting the molar ratios of O-TPA and Cl-TPA. For example, changing the O-TPA/Cl-TPA ratio from 2:1 to 1:2 led to the thickness of the upper part decreasing from 90 μm to 55 μm, while the thickness of the lower part increased from 70 μm to 96 μm (Fig. 2e and Fig. S33 in Supporting information).

Asymmetric wettability of the Janus COF membrane was demonstrated by water contact angle (WCA) measurements (Fig. 3a). The Janus membrane exhibited a remarkable difference in WCA between its upper surface (<5°) and lower surface (133.3°). In contrast, this phenomenon was not observed for the two-component COF membrane of LY-QH, which showed WCA of 49.9° and 59.9° for the upper and lower surfaces, respectively. A surprising phenomenon was observed for LY-SH. The water contact angles of the upper and lower surfaces of LY-SH were measured to be 73.7° and 120.4°, respectively, indicating a certain degree of asymmetric wettability. Different from the result of LY-QH, the asymmetric wettability of LY-SH was obtained by serendipity, which could not be designed and predicted because both the upper and lower surfaces of this membrane have the same chemical constitution. The different outcomes of LY-QH and LY-SH again manifests that the conventional two-phase interfacial polymerization cannot provide precise control over the wettability of the membranes in preparation, and is hard to design and predict asymmetric wettability of a membrane on the basis of this method. Moreover, underwater oil contact angle (UOCA) measurements conducted for the upper surface of LY-Janus further corroborate the asymmetric wettability of the Janus membrane, which showed UOCA of 124.5° ± 0.4° for five different types of oils (Fig. 3b). WCA under varying pH conditions was further measured for the lower surface. Angles of 132.9° ± 0.7° were obtained at 7 different pH values (Fig. 3c). These results clearly demonstrate the Janus feature of the membrane and its universal asymmetric wettability.

Next, antifouling capability of the Janus membrane was assessed by ejecting water (or oil) to its surfaces when the membrane was immersed in oil (or water). It was observed that water droplets (dyed with Direct Red 28 for naked-eye observation) readily slid off the hydrophobic surface immersed in dichloromethane, while toluene droplets (dyed with Solvent Blue 104) quickly slid away from the hydrophilic surface immersed in water (Fig. S34 and videos S1 and S2 in Supporting information), showcasing an excellent antifouling property. The anti-fouling performance of the LY-Janus membrane was further evaluated through cyclic tests alternating between O/W emulsion separation and water permeability measurements. Dynamic light scattering (DLS) analysis confirmed efficient emulsion separation with a significant reduction in droplet size after each cycle. The membrane maintained stable water flux and complete separation efficiency over five consecutive cycles, demonstrating its remarkable anti-fouling capability and long-term operational stability (Figs. S35 and S36 in Supporting information). Moreover, the opposite wettability between the two sides of the Janus membrane should contribute to a unique unidirectional water transport characteristic (Fig. 4a), which was proposed to be a result of response to multiple pressure [24,26–28]. To investigate this behavior, LY-Janus was affixed in the middle of an H-type cell which contains a small amount of Direct Red 28 dye in one side and water in the other side (Fig. 4b). In contrast to the COF membranes LY-QH and LY-SH for which water could free pass from both the upper and lower sides, LY-Janus exclusively permits water to transport from the hydrophobic surface (lower side) to the hydrophilic surface (upper side), while effectively blocks the reverse direction, demonstrating a behavior similar to the function of a diode. The above processes were also monitored by videos, which clearly showed dramatic difference between the membranes LY-Janus and LY-QH and LY-SH, as well as the unidirectional water transport (Videos S3-S8 in Supporting information). Additionally, as shown in Fig. 4c, water droplet with the volume of 1 μL penetrated the LY-Janus membrane from the hydrophobic side to the hydrophilic side within approximately 75 s, whereas the similar phenomenon was not observed for the LY-SH and LY-QH membranes, further confirming unidirectional transport capability of the Janus membrane. Notably, the Janus membrane exhibited a high durability. It could maintain its performance on the unidirectional water transport over 20 cycles without any deterioration (Fig. 4d). The longevity underscores potential of the membrane for sustained and repeated use during practical applications, thanks to its monolithic structure. To characterize the diode-like behavior of the LY-Janus membrane, additional quantitative experiments were conducted to measure flux-pressure curves. As shown in Fig. S37 (Supporting information), under a pressure range of 0–2.0 bar, the LY-Janus membrane exhibits stable water flux when

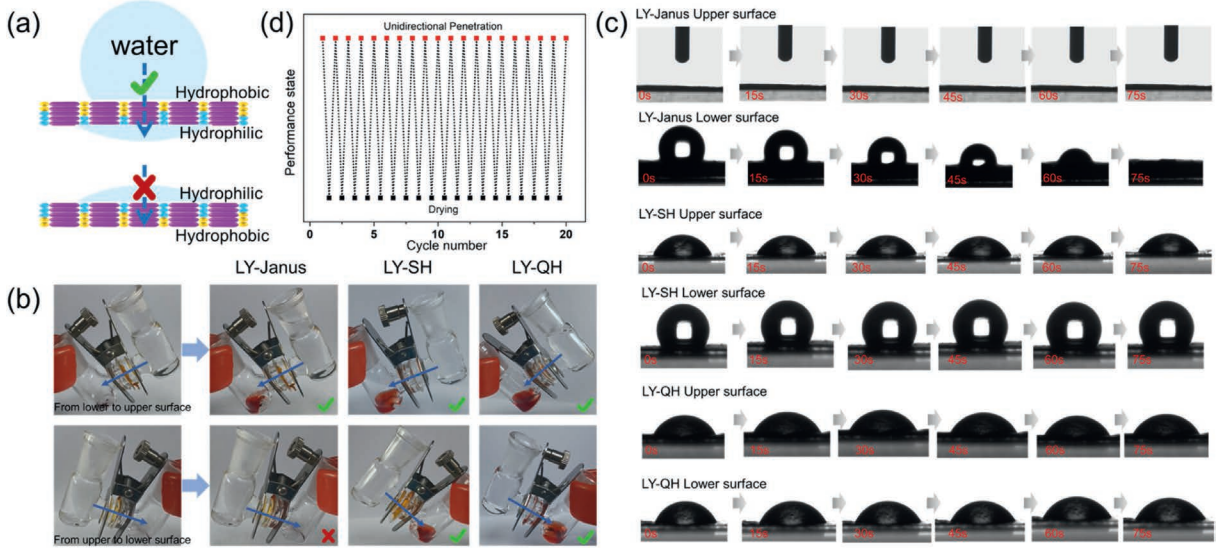


Fig. 4. (a, b) Schematic diagram and experimental results of unidirectional water transport. (c) Penetration process of water droplets on the surfaces of the LY-Janus, LY-SH, and LY-QH membranes, with the red numbers indicating their residence time. (d) Cycle stability of unidirectional water transport.

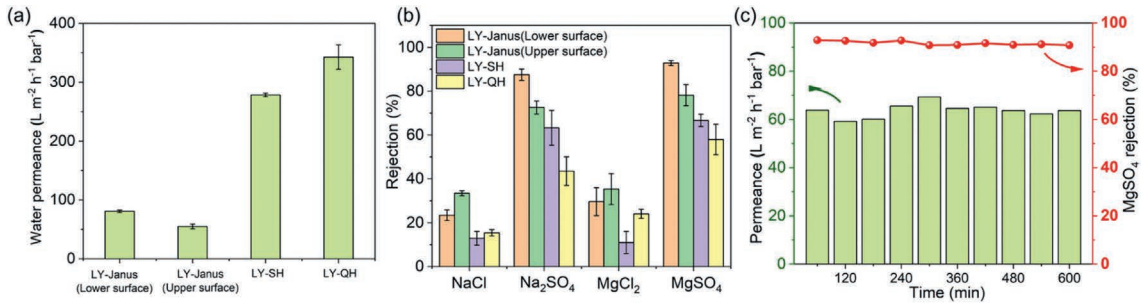


Fig. 5. (a, b) Water flux and performance of the LY-Janus (lower surface and upper surface), LY-SH and LY-QH membranes in filtrating different salts. (c) Impact of operation time on nanofiltration performance of the LY-Janus membrane (lower surface) (Note: concentration of the salts is 1000 ppm and operation pressure is 1 bar).

permeating from the hydrophobic side to the hydrophilic side. In contrast, no water permeation is observed when the direction is reversed, until the pressure exceeds 0.6 bar. Beyond this threshold, flux increases with pressure, and further pressure elevation leads to membrane failure. These results suggest a breakthrough pressure between 0.6 and 0.8 bar. This distinct behavior reflects the diode-like property of the membrane, in accordance with the asymmetric wetting of the Janus structure.

Practical application of the as-prepared Janus COF membrane was exploited. To this end, nanofiltration performance of the membranes was evaluated *via* water flux and filtration experiments using 1000 ppm aqueous solutions of NaCl, Na_2SO_4, $MgCl_2$, and $MgSO_4$, respectively. As shown in Fig. 5a, the water fluxes measured for the LY-Janus lower surface (from the hydrophobic surface to the hydrophilic surface), LY-Janus upper surface (from the hydrophilic surface to the hydrophobic surface), LY-SH, and LY-QH were 81, 55, 278 and 343 L m^{-2} h^{-1} bar^{-1}, respectively. Although LY-Janus (from the hydrophobic surface to the hydrophilic surface) exhibited a lower permeance flux relative to LY-SH and LY-QH, it demonstrated significantly higher retention, achieving rejections of 87.5 % and 92.9 % for Na_2SO_4 and $MgSO_4$, respectively (Fig. 5b). Moreover, the rejections for Na_2SO_4 and $MgSO_4$ were considerably higher than those for $MgCl_2$ and NaCl, possibly due to a synergistic effect of size-sieving with sulfate salts [65–67]. Notably, adjusting the equivalence ratio of O-TPA to Cl-TPA enables precise control over the thicknesses of the hydrophilic and hydrophobic layers, thereby balancing the trade-off between flux and selectivity in the LY-Janus membrane (Fig. S38 in Supporting information). To further elucidate the separation mechanism, the separation performance of the LY-Janus membrane is attributed to the synergistic contributions of molecular sieving and Donnan exclusion. The rejection behavior toward dyes with varying molecular sizes was analyzed, yielding an estimated mean effective pore size of approximately 0.8 nm and a corresponding pore size distribution derived from the rejection data (Fig. S39 in Supporting information). The smaller experimental pore size, compared to the non-local density functional theory (NLDFT) prediction, arises from the staggered arrangement of alkyl and alkoxy side chains in the COF channels. This arrangement diminishes the accessible pore volume, resulting in an improvement in size-selective ion sieving. Moreover, the membrane possesses a negative surface potential of −38.67 mV at pH 7 (Fig. S40 in Supporting information). This electronegativity facilitates anion exclusion through the Donnan effect, thereby contributing to enhanced overall separation efficiency. Furthermore, when conducting nanofiltration through the lower surface, the LY-Janus membrane maintained stable $MgSO_4$ rejection (>90 %) and permeance (~60 L m^{-2} h^{-1} bar^{-1}) over a long continuous nanofiltration process (Fig. 5c). However, nanofiltration through the upper surface of LY-Janus resulted in notable defects following pressure breakthrough (Fig. S41 in Supporting information). SEM study further corroborated this observation, revealing substantial structural damage (Fig. S42 in Supporting information). This stability was attributed to the unique capability of Janus membrane endowed by the unidirectional water transport.

In summary, by developing a multiphase interfacial polymerization strategy, we successfully fabricated three-component Janus COF membranes with opposite wettability on their two surfaces. The membranes are monolithic and free-standing, exhibiting robust anti-pollution capability. Furthermore, in comparison with the two-component COF membranes constructed *via* traditional two-phase interfacial polymerization method, the Janus COF membranes showcases a unique unidirectional water transport characteristic, which efficiently transports water from the hydrophobic surface to the hydrophilic surface. This design also achieves high retention of $MgSO_4$ (>90%) and maintains stable performance across many testing cycles for nanofiltration. The method developed in this study provides a facile and general way for designable, predictable, and controllable fabrication of COF membranes with asymmetric properties, opening new possibilities for their diverse structures and applications. It can also serve as a valuable reference for the construction of heterogeneous/asymmetric membranes from different types of materials, with more potentials to be explored.

CRediT authorship contribution statement

Ya Lu: Writing – original draft, Data curation, Conceptualization. **Chao Jia:** Data curation. **Shu-Yan Jiang:** Data curation. **Qiao-Yan Qi:** Software, Data curation. **Jin Yao:** Writing – review & editing, Funding acquisition, Conceptualization. **Xin Zhao:** Writing – review & editing, Supervision, Resources, Project administration, Funding acquisition, Conceptualization.

Declaration of competing interest

The authors declare that they have no known competing financial interests or personal relationships that could have appeared to influence the work reported in this paper.

Acknowledgments

We thank the National Natural Science Foundation of China (Nos. 22101063 and 21725404) and the Strategic Priority Research Program of the Chinese Academy of Sciences (No. XDB0610000) for financial support.

Supplementary materials

Supplementary material associated with this article can be found, in the online version, at doi:10.1016/j.cclet.2025.112307.

References

[1] H. Bellanger, T. Darmanin, E. Taffin de Givenchy, et al., Chem. Rev. 114 (2014) 2694–2716.
[2] Z. Li, Z. Guo, Nanoscale 11 (2019) 22636–22663.
[3] Q. Sun, D. Wang, Y. Li, et al., Nat. Mater. 18 (2019) 936–941.
[4] H. Chen, P. Zhang, L. Zhang, et al., Nature 532 (2016) 85–89.
[5] Y. Wang, S. Gao, W. Xu, et al., Adv. Funct. Mater. 30 (2020) 1908252.
[6] J. Chen, Z.X. Low, S. Feng, et al., ACS Appl. Mater. Interfaces 13 (2021) 60763–60788.
[7] K. Yin, H. Du, X. Dong, et al., Nanoscale 9 (2017) 14620–14626.
[8] Y. Hou, C. Duan, G. Zhu, et al., J. Membr. Sci. 591 (2019) 117312.
[9] Y. Yin, W. Wang, A.K. Kota, et al., Environ. Sci.: Water Res. Technol. 5 (2019) 2004–2014.
[10] X.Y. Guo, L. Zhao, H.N. Li, et al., Science 386 (2024) 654–659.
[11] H. Fashandi, A.R. Ghomi, Adv. Eng. Mater. 19 (2017) 1600863.
[12] H.C. Yang, J. Hou, V. Chen, et al., Angew. Chem. Int. Ed. 55 (2016) 13398–13407.
[13] M. Afsari, H.K. Shon, L.D. Tijing, Adv. Colloid Interface Sci. 289 (2021) 102362.
[14] H. Zhou, Z. Guo, J. Mater. Chem. A 7 (2019) 12921–12950.
[15] L. Yan, X. Yang, Y. Zhang, et al., Mater. Today 51 (2021) 626–647.
[16] H.N. Li, J. Yang, Z.K. Xu, Adv. Mater. Interfaces 7 (2020) 1902064.
[17] H.C. Yang, Y. Xie, J. Hou, et al., Adv. Mater. 30 (2018) 1801495.
[18] R. Zhang, Y. Sun, Z. Guo, et al., Adv. Sustainable Syst. 5 (2021) 2000253.
[19] M. Cao, J. Xiao, C. Yu, et al., Small 11 (2015) 4379–4384.
[20] H.C. Yang, W. Zhong, J. Hou, et al., J. Membr. Sci. 523 (2017) 1–7.
[21] Y.X. Huang, Z. Wang, J. Jin, et al., Environ. Sci. Technol. 51 (2017) 13304–13310.
[22] S. Liu, C. Wu, W.S. Hung, et al., J. Mater. Chem. A 5 (2017) 22988–22996.
[23] C. Yang, N. Han, C. Han, et al., ACS Appl. Mater. Interfaces 11 (2019) 22408–22418.
[24] X. Li, W. Zhang, R. Qu, et al., J. Mater. Chem. A 7 (2019) 10047–10057.
[25] X. Yang, L. Yan, F. Ran, et al., J. Membr. Sci. 576 (2019) 9–16.
[26] J. Wu, N. Wang, L. Wang, et al., Soft Matter 8 (2012) 5996–5999.
[27] L. Hu, S. Gao, Y. Zhu, et al., J. Mater. Chem. A 3 (2015) 23477–23482.
[28] L. Cao, I.C. Chen, X. Liu, et al., ACS Nano 16 (2022) 18910–18920.
[29] X. Chen, K. Geng, R. Liu, et al., Angew. Chem. Int. Ed. 59 (2020) 5050–5091.
[30] P.J. Waller, F. Gándara, O.M. Yaghi, Acc. Chem. Res. 48 (2015) 3053–3063.
[31] R.R. Liang, S.Y. Jiang, R.H. A, et al., Chem. Soc. Rev. 49 (2020) 3920–3951.
[32] J. Yao, Y. Lu, H. Sun, et al., Chem. Res. Chin. Univ. 38 (2022) 364–372.
[33] G. He, R. Zhang, Z. Jiang, Acc. Mater. Res. 2 (2021) 630–643.
[34] S. Yuan, X. Li, J. Zhu, et al., Chem. Soc. Rev. 48 (2019) 2665–2681.
[35] C. Wang, H. Xie, R. Xia, et al., Chin. Chem. Lett. 36 (2025) 110642.
[36] Y. Wang, H. Wang, Y. Liu, et al., Chin. Chem. Lett. 36 (2025) 110189.
[37] Y. Ying, S.B. Peh, H. Yang, et al., Adv. Mater. 34 (2022) 2104946.
[38] X. Shi, Z. Zhang, C. Yin, et al., Angew. Chem. Int. Ed. 61 (2022) e202207559.
[39] Z. Liang, B. Liang, L. Gong, et al., Chin. J. Chem. 41 (2023) 2425–2431.
[40] S. Ai, Y. Xu, H. Zhou, et al., Chin. Chem. Lett. 36 (2025) 110761.
[41] Y. Wu, Y. Wang, F. Xu, et al., J. Membr. Sci. 659 (2022) 120799.
[42] R. Dong, T. Zhang, X. Feng, Chem. Rev. 118 (2018) 6189–6235.
[43] W. Xian, P. Zhang, C. Zhu, et al., CCS Chem. 3 (2021) 2464–2472.
[44] R. Wang, X. Shi, A. Xiao, et al., J. Membr. Sci. 566 (2018) 197–204.
[45] K. Dey, M. Pal, K.C. Rout, et al., J. Am. Chem. Soc. 139 (2017) 13083–13091.
[46] H. Wang, Z. Zeng, P. Xu, et al., Chem. Soc. Rev. 48 (2019) 488–516.
[47] Z. Wang, S. Zhang, Y. Chen, et al., Chem. Soc. Rev. 49 (2020) 708–735.
[48] D.W. Burke, Z. Jiang, A.G. Livingston, et al., Adv. Mater. 36 (2024) e2300525.
[49] L. Zhou, X. Li, K. Cao, et al., Adv. Funct. Mater. 32 (2022) 2108178.
[50] S. Jia, L. Hao, Y. Liu, et al., ACS Mater. Lett. 5 (2023) 458–465.
[51] S. Mohata, K. Dey, S. Bhunia, et al., J. Am. Chem. Soc. 144 (2022) 400–409.
[52] X. Wang, B. Shi, H. Yang, et al., Nat. Commun. 13 (2022) 1020.
[53] Y. Lu, C. Jia, S.Y. Jiang, et al., ChemRxiv (2024), doi:10.26434/chemrxiv-2024-s2kf2.
[54] A. Puthukkudi, S. Nath, P. Shee, et al., Adv. Mater. 36 (2024) 2312960.
[55] S.Y. Jiang, Z.B. Zhou, S.X. Gan, et al., Nat. Commun. 15 (2024) 698.
[56] R. Yang, S. Liu, Q. Sun, et al., J. Am. Chem. Soc. 144 (2022) 11778–11787.
[57] B. Li, Y. Cheng, X. Ma, et al., Chin. Chem. Lett. 37 (2026) 111134.
[58] C. Liu, C. Jia, S.X. Gan, et al., Chin. Chem. Lett. 35 (2024) 109750.
[59] L. Cusin, P. Cieciórski, S. Van Gele, et al., Nat. Synth. 4 (2025) 632–641.
[60] L. He, L. Wang, Z. He, et al., Chin. Chem. Lett. 36 (2025) 110717.
[61] Z.F. Pang, T.Y. Zhou, R.R. Liang, et al., Chem. Sci. 8 (2017) 3866–3870.
[62] L.M. Lanni, R.W. Tilford, M. Bharathy, et al., J. Am. Chem. Soc. 133 (2011) 13975–13983.
[63] R.L. Li, A. Yang, N.C. Flanders, et al., J. Am. Chem. Soc. 143 (2021) 7081–7087.
[64] S. Zhao, C. Jiang, J. Fan, et al., Nat. Mater. 20 (2021) 1551–1558.
[65] X. Liu, J. Wang, Y. Shang, et al., J. Am. Chem. Soc. 146 (2024) 2313–2318.
[66] S. Maiti, S.S. Islam, S. Bose, Environ. Sci.: Water Res. Technol. 9 (2023) 249–264.
[67] Y. Li, Q. Wu, X. Guo, et al., Nat. Commun. 11 (2020) 599.